Heliyon 9 (2023) e20200

Contents lists available at ScienceDirect

Heliyon

journal homepage: www.cell.com/heliyon

Optimization of tetrastigma hemsleyanum extraction process based on GA-BPNN model and analysis of its antioxidant effect

Jianhao Shu [a,1], Yali Zhao [b,1], Yehui Zhou [c], Feifei Lin [b], Jingmei Song [d,*], Xiaohong Li [c,**]

[a] The Second Clinical Medical College, Zhejiang Chinese Medical University, Hangzhou, 310051, China
[b] College of Life Science, Zhejiang Chinese Medical University, Hangzhou, 310051, China
[c] College of Pharmaceutical Science, Zhejiang Chinese Medical University, Hangzhou, 310051, China
[d] College of Basic Medical Science, Zhejiang Chinese Medical University, Hangzhou, 310051, China

ARTICLE INFO

Keywords:
Genetic algorithm-back propagation neural network
Box-behnken design
Optimization of the extraction process
Network pharmacology
Antioxidant activity

ABSTRACT

Tetrastigma hemsleyanum (*Tetrastigma hemsleyanum* Diels et Gilg) is a valuable traditional Chinese medicine with various applications. In this study, we aimed to optimize the extraction process for the total extraction yield of five flavonoid components, namely kaempferol, quercetin, rutin, kaempferol-3-O-rutinoside, and astragalin from the *Tetrastigma hemsleyanum* root (THR), and explore its potential molecular mechanisms in treating oxidative diseases as well as antioxidant activity. To achieve these objectives, we employed the genetic algorithm-back propagation neural network (GA-BPNN), the Box-Behnken design (BBD) with 4-factors and 3-levels to establish the optimal ethanol extraction process for the total extraction yield of the 5 components. Using public databases, the "component core targets-disease core target genes" networks were built, as well as molecular docking. Furthermore, DPPH was used to examine the antioxidant activity of the extracts obtained from THR under the optimal extraction process. The experimental value of the total extraction yield of the 5 components achieved a maximum of 788.12 mg/kg when the ethanol concentration was 73%, the solid-liquid ratio was 26 g/mL, and the ultrasonic duration was 30 min, and the ultrasonic temperature was 76 °C. When docked with protein molecules such as 6Y8I, quercetin, and other components received moderate to high scores. When the total concentration of the 5 components was 3.033 μg/mL, the DPPH radical scavenging rate was 89.81%. Compared with the BBD method, the GA-BPNN method is more efficient and reliable for optimizing the extraction process of active ingredients in THR because of its good data-fitting ability.

1. Introduction

Tetrastigma hemsleyanum Diels et Gilg (Vitaceae), commonly known as shefuzi, jinqiandiaohulu, and tujingwan, is a perennial

* Corresponding author.
** Corresponding author.
E-mail addresses: jianhao_shu@126.com (J. Shu), zhaoyali2002@126.com (Y. Zhao), zyehui_519@163.com (Y. Zhou), linfeifei0806@163.com (F. Lin), songjingmei1983@163.com (J. Song), li_xiaoh2005@163.com (X. Li).
[1] These authors contributed equally to this work and should be considered co-first authors.

https://doi.org/10.1016/j.heliyon.2023.e20200
Received 15 June 2023; Received in revised form 12 September 2023; Accepted 13 September 2023
Available online 22 September 2023

evergreen herbaceous trailing vine [1]. The *T. hemsleyanum* root (THR, called "Sanyeqing" in Chinese) is a functional food that is widely utilized in China. It is often consumed as a functional tea or dietary supplement as an edible plant. THR is slightly bitter and moderate, with the effects of clearing heat and detoxifying, anti-inflammatory and pain-relieving, dispelling wind and phlegm, and can treat pneumonia, asthma, hepatitis, menstrual disorders, lymphatic tuberculosis, and febrile convulsions in children, according to the ancient Chinese medical texts [2,3]. THR is mainly composed of compounds such as flavonoids, terpenoids, and volatile oils [3]. Flavonoids are the primary cause of the biological activities mentioned above, and their components have good anti-inflammatory and anti-tumor effects [4,5]. Kaempferol has been proven in modern pharmacological studies to have antioxidant properties [6], as well as the ability to treat hepatocellular carcinoma [7], breast cancer [8], and other diseases. It can also be used as a dietary supplement to maintain antioxidant enzymes active by scavenging free radicals, delaying the onset and progression of neurodegenerative diseases [9]. In clinical settings, quercetin has been demonstrated to have multifaceted anti-inflammatory and thrombin-inhibiting effects, and it has been proven that quercetin in combination with kaempferol as a dietary supplement can better promote cardiovascular circulation [1,10–13]. Rutin possesses anti-inflammatory, antioxidant, anti-diabetic, and neuroprotective pharmacological effects [14]. Kaempferol-3-O-rutinoside exhibits pharmacological effects such as neuroprotection, lung adenocarcinoma inhibition, and hepatoprotection [15–17]. Astragalin possesses anti-inflammatory, cardioprotective, anti-obesity, and anti-osteoporosis effects [18].

Most current THR studies focus on components such as polysaccharide extracts [19], and there are relatively few studies on flavonoid extraction and antioxidant activity *in vivo* and in vitro; however, the potential antioxidant properties of dietary flavonoids have received much attention in recent years. Due to the limitations of the traditional response surface methodology (RSM), several researchers have developed genetic algorithm-back propagation neural network (GA-BPNN) models to optimize the extraction of active ingredients in Chinese medicine [20,21]. As a result, optimizing the extraction process of THR flavonoid components and studying network pharmacology on the antioxidant activity can not only provide a novel idea for the study of THR's pharmacological mechanism but also have important implications for future research on THR's antioxidant mechanism.

Based on single-factor experiments, the Box-Behnken design (BBD) and GA-BPNN model were used to predict the optimal extraction process of total extraction yield of 5 flavonoid index components in THR: kaempferol, quercetin, rutin, kaempferol-3-O-rutinoside, and astragalin. The network pharmacology was applied to find the relationship between the 5 components and oxidative disease targets *in vivo* and pairing with related proteins. Moreover, THR extracts under optimal extraction conditions were employed to perform DPPH antioxidant activity assay. This work aims to strengthen THR's alternative role to traditional drugs in the treatment of oxidative diseases, provide a reference for further research on the mechanisms related to the *in vivo* antioxidant activity of flavonoid components in THR, improve THR's scientific and economic value and promote the development and upgrading of related industries.

2. Materials and methods

2.1. Instruments

DFY-500Herbal Crusher (Wenling City Linda Machinery Co.); AL104Microbalance (Mettler Toledo Instruments (Shanghai) Co.); XP105DR Precision analytical balance (Mettler Toledo Instruments, Switzerland Ltd.); SK5210HP Ultrasonic Cleaner (Shanghai Kudos Ultrasonic Instrument Co.); Eppendorf 5430 r Centrifuge (Eppendorf AG, Germany); Spectra Max Plus384Absorbance microplate reader (American Molecular Devices, Inc.); Waters-e2695 High-Performance Liquid Chromatograph with 2489 UV/Vis Detector (Waters Corporation, USA).

2.2. Materials and chemicals

2.2.1. Plant materials

The THR (Batch no. 10896–6754) was purchased from the Zhejiang Hospital of Traditional Chinese Medicine and identified by Prof. *Wu Qiaofeng* of the Zhejiang Chinese Medicine University as the dried root tuber of *T. hemsleyanum*, a climbing vine. The roots were dried and sealed before the experiment, bagged, and stored in a dark room.

2.2.2. Reference substances

The reference substances of rutin (Batch No. 1000080–200707), kaempferol-3-O-rutinoside (Batch No. 21070121), astragalin (Batch No. DSTDZ000101), kaempferol (Batch No. C15H1006), and quercetin (Batch No. C15H1007) were purchased from Chengdu Destructive Co (Chengdu, China) and their purity was $\geq$98% according to HPLC area normalization.

2.2.3. Chemical reagents

Ethanol; 0.1% formic acid (analytical grade purity); ultrapure water; acetonitrile (chromatographic grade purity); methanol; DPPH; VC. Major chemical reagents, including DPPH, were obtained from Shanghai Biochemical Co., Ltd. (Shanghai, China).

2.3. Sample preparation

An adequate amount of dried THR tuber was taken, crushed using an herb crusher, and then sifted through a 20-mesh sieve. The crude THR powder was meticulously weighed at 3.0 g using a microbalance. Subsequently, 75 mL of 50% ethanol was introduced, and its weight was recorded. Ultrasonic treatment was conducted at 40 °C with an ultrasonic frequency of 53 kHz for a duration of 45 min.

After cooling to room temperature and reweighing precisely, any lost weight was compensated for by adding 50% ethanol. The resulting mixture was thoroughly shaken, followed by centrifugation. The supernatant was then filtered through a 0.45 μm microporous membrane.

On a precision analytical balance, an appropriate amount of each reference substance was weighed, and methanol was added to form a mixed control solution comprising 0.530 mg rutin, 1.545 mg kaempferol-3-O-rutinoside, 0.160 mg astragalin, 0.080 mg quercetin, and 0.064 mg kaempferol per 10 mL.

2.4. Chromatographic conditions

High performance liquid chromatograph, column: ZORBAX SB-C18 (250 mm × 4.6 mm, 5 μm); mobile phase: 0.1% formic acid solution (A)-acetonitrile (B), formic acid solution should be ultrasonicated in advance under ultrasonic cleaner, gradient elution program: 0–10 min, 90–85% A; 10–15 min, 85–77% A; 15–17 min, 77–72% A; 17–23 min, 72% A; 23–30 min, 72–62% A; 30–35 min, 62–62% A detection wavelength: 360 nm; column temperature: 25 °C; flow rate: 1.0 mL/min injection volume: 10 μL.

2.5. Experimental design

2.5.1. Single-factor experiments

The extraction solvent was ethanol, and the ultrasonic power was 120 W. Important parameters were particle size (mesh), ethanol concentration (%), solid-liquid ratio (g/mL), ultrasonic duration (min), and ultrasonic temperature (°C). The THR powder was precisely weighed at 50.0 mg, and the initial conditions were 20 mesh, 50% ethanol concentration, 1:25 g/mL solid-liquid ratio, 45 min sonication, and 50 °C sonication temperature. The particle size was examined as not sieved, above 10, 20, 30, 50, 80 mesh, powder (>100 mesh), the ethanol concentration was 20%, 40%, 50%, 60%, 80%, 100%, the solid-liquid ratio was 1:10, 1:15, 1:20, 1:25, 1:30, 1:35 g/mL. The ultrasonic duration was 15, 30, 45, 60, 75, and 90 min, respectively, and the ultrasonic temperature was 30, 40, and 50 °C, respectively. The peak areas of the 5 components of THR were recorded, and the contents of the 5 components were using equation (1), and each experiment was repeated thrice in parallel.

$$x_i = \frac{S_{si} \times V}{S_{ci} \times C_{ci}} \tag{1}$$

where, x_i is the content of each component (mg); S_{si} and S_{ci} are the peak areas of the sample and control of each component, respectively; V is the volume of THR extract (mL); C_{ci} is the concentration of the control of each component (mg/mL).

The total extraction yield of the 5 components can be obtained from equation (2):

$$D = \sum_{i=1}^{5} \frac{x_i \times 10^6}{M} \tag{2}$$

where D is the total extraction yield of the 5 components (mg/kg); M is the mass of THR in each group (mg).

The range of optimal levels of the 5 components can be first calculated based on the quantity of total extraction yield.

2.5.2. BBD

The significant factors affecting the total extraction yield of the 5 components of THR and the individual levels of each factor were identified based on the results of the single-factor experiments, and the total extraction yield was used as the response value, and the combined experiments were designed and arranged using Design-Expert 8.0.6 software, and each group was measured thrice in parallel and the mean values were taken. The combined experiment findings were statistically analyzed using a two-sided significance test $p < 0.05$, and all experimental results data were expressed as mean ± standard deviation ($\bar{x} \pm s$).

2.6. Model and optimization

2.6.1. Modeling by RSM

Using RSM on the experimental data of BBD, a quadratic polynomial regression equation is established, as shown in equation (3),

$$Y = \beta_0 + \sum_{i=1}^{n} \beta_i X_i + \sum_{i=1}^{n} \sum_{j \geq 1}^{n} \beta_{ij} X_i X_j + \varepsilon \tag{3}$$

where, Y represents the response variable; X_i represents the independent variable i ($i = 1,2, \ldots,n$); β_0 is the constant term; β_i ($i = 1,2,3,4$) represents the coefficient of the primary term; β_{ij} ($i, j = 1,2,3,4$) represents the coefficient of the second term, and ε represents the residual between the experimental value and the model estimate.

Analysis of variance (ANOVA) was performed to determine the significance of each component in the regression equation and to assess whether there was a linear relationship between them and the dependent variable to determine whether the regression equation was significant. When $p < 0.05$ ($\alpha = 0.05$) was attained, the regression equation was deemed statistically significant.

2.6.2. Modeling by GA-BPNN and optimization

Back propagation neural network (BPNN), a simplified computational model inspired by the structure of biological neural networks, consists of an input layer, a hidden layer, and an output layer. Fig. 2 depicts a neural network with 3 layers. The relationship among neurons in two adjacent layers can be expressed as equation (4):

$$\begin{cases} S_j = f\left(\sum_{i=1}^{4} W_{ij}{}^{(1)} X_i + b_j{}^{(1)}\right), j = 1, 2, \ldots, n \\ Y = g\left(\sum_{j=1}^{n} W_j{}^{(2)} S_j + b^{(2)}\right) \end{cases} \tag{4}$$

where f is the sigmoid activation function and g is the purelin activation function; $W_{ij}^{(1)}$ and $W_{ij}^{(2)}$ are the network weights; $b_j^{(1)}$ and $b^{(2)}$ are the bias values; X_i is the input variable and S_j and Y denote the output variables of the hidden layer and output layer, respectively.

The genetic algorithm (GA) is a global optimization search algorithm that simulates the biological evolution process. The population is generated first, and then transformed into a binary code; the fitness function is set to evaluate the merit of individuals in the population; the population then simulates the biological genetic process, and after selection, crossover, and mutation, the superior individuals are obtained and inherited to the next generation; iterations are repeated until the termination condition is reached, at which time the individual is the optimal solution.

To investigate the topic of extracting process condition preferences, genetic neural networks integrate the BPNN model with the GA optimization function. The GA's global optimization-seeking function is used to optimize the structure of the neural network and the network parameters, and the global optimal solution is found using the global optimization-seeking function, and the flow of the GA-BPNN is shown in the literature [22].

2.7. Network pharmacology study of THR

The keywords of 5 flavonoid components were entered into the TCMSP database (https://old.tcmsp-e.com/index.php). Kaempferol, quercetin, rutin, kaempferol-3-O-rutinoside, astragalin, and related targets were obtained in "Related Targets" and incorporated. To acquire the corresponding targets, the UniProt database (https://www.uniprot.org/) was utilized, and "Homo sapiens" and "reviewed" targets were selected. The target name obtained from the TCMSP database was then transformed and de-duplicated.

To obtain oxidation-related disease targets, the gene cards (https://www.genecards.org/), OMIM (https://omim.org/), and PharmGKB (https://www.pharmgkb.org/) databases were searched with "oxidant" as the keyword, and the related disease target genes were retrieved after collation.

The R language program's Venn package was used to plot Venn diagrams and locate the intersections of 5 components with disease targets. The intersecting genes were imported into the STRING database (https://cn.string-db.org/), the lowest interaction value with high confidence (0.7) was chosen, unlinked nodes were hidden, and PPI files were obtained for analysis. The downloaded files were imported into the Cytoscape_v3.9.0 software for analysis, and the cytoNCA extension was used to calculate betweenness (BC), closeness (CC), degree (DC), eigenevector (EC), local average connectivity-based method (LAC), and network (NC) values (all without weights). The higher the value obtained, the more central the node in the PPI network. The genes above the median value are considered core targets.

Using the bioconductor packages of the R language program, the gene symbols of the overlapping targets of the 5 flavonoid components with oxidation-related diseases were converted into entrez ID for enrichment analysis. After that, KEGG enrichment and GO enrichment analyses were performed using the relevant packages of the R language program, with a significance threshold set at p-value <0.05. In KEGG enrichment, the top 30 items of the enrichment results were chosen, and bar and bubble plots were drawn using the R language program; in GO enrichment, the top 10 items of biological process (BP), cellular components (CC), and molecular function (MF) were selected, and the bar and bubble plots were drawn.

The 2D chemical structure formulae for each of the 5 components were retrieved from the PubChem database, and the molecules were energy minimized using Chem3D software. The gene names were searched in the PDB database, screened by X-ray Diffraction with Homo sapiens, and the corresponding proteins were selected and downloaded. The SYBYL-X 2.0 software was used to remove water and add hydrogen to the proteins. Subsequently, the molecular docking was executed, guided by the docking fraction criteria: 3–5 indicating moderate activity and >5 signifying higher activity).

2.8. Antioxidant activity

A microbalance was used to precisely weigh DPPH 0.8 mg and VC 3.0 mg. The former was dissolved in anhydrous ethanol and fixed into a 10 mL brown volumetric flask, then 100 μL was taken from the brown volumetric flask and diluted 10 times to make an 8 μg/mL DPPH solution, stored away from light and set aside; the latter was dissolved in pure water and fixed into a 10 mL volumetric flask, then 100 μL was taken from the volumetric flask and similarly diluted 10 times and shaken well to obtain a 0.03 mg/mL VC solution. Take 0.5 mL of each VC solution and dilute it 1, 2, 4, 6, 8, 10, 16, 32, 64, 100, 128, and 256 times to make concentrations of 0.01, 0.02, 0.03, 0.05, 0.09, 0.19, 0.30, 0.38, 0.51, 0.76, 1.52, and 3.03 μg/mL of VC standard test solution, shake well, keep away from direct light and set aside.

The THR extracts under the optimal extraction process were used as the THR group. To fix the volume, an appropriate amount of

the THR extracts was added to a certain amount of ethanol (ethanol concentration under optimal extraction conditions), shaken well, and left to stand. At room temperature and in the absence of light, the absorbance (A_i) was measured for 10 min at 517 nm 100 μL was added to 100 μL of anhydrous ethanol, mixed well, and the absorbance (A_j) was measured at 517 nm for 10 min at room temperature

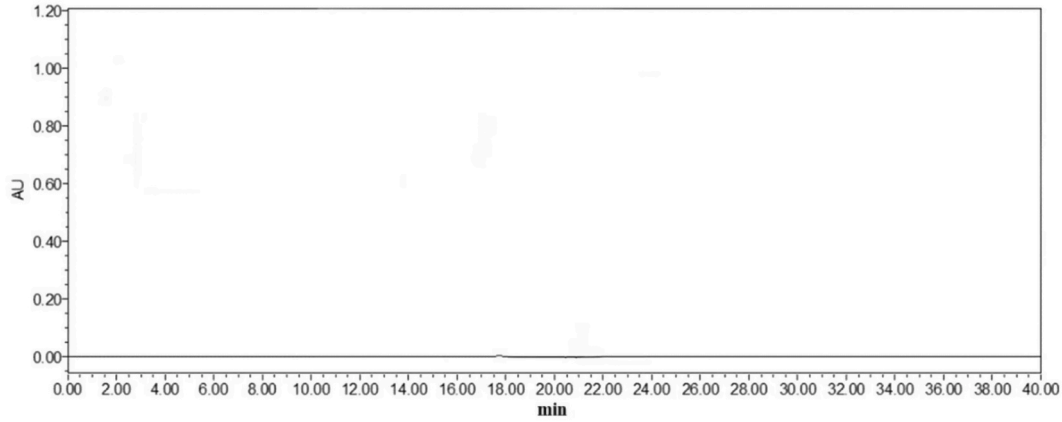

(a)

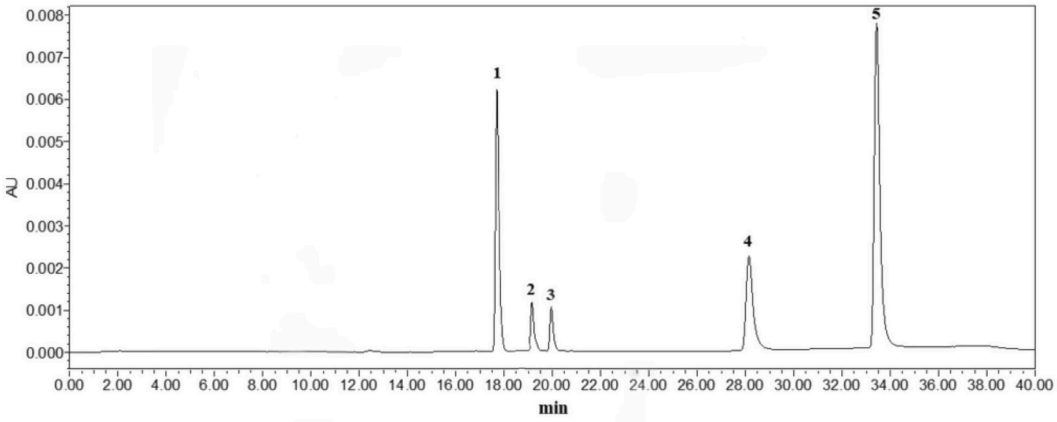

(b)

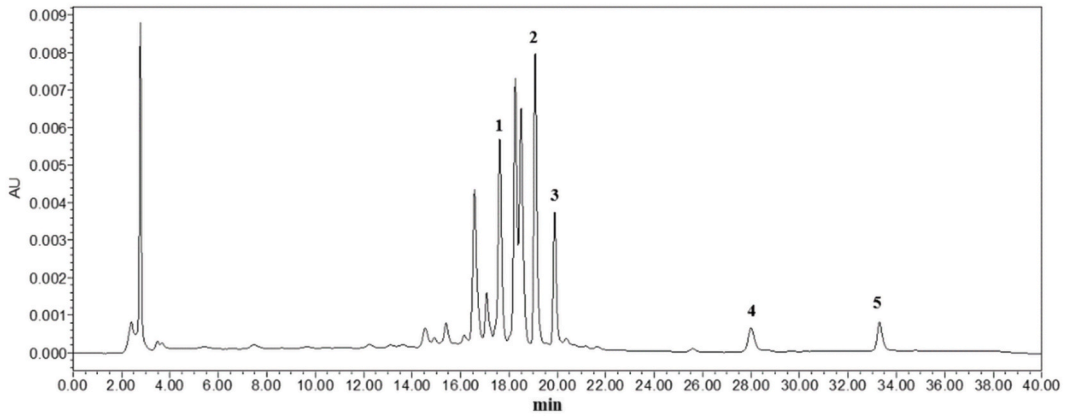

(c)

Fig. 1. HPLC chromatogram (a-c): (a) negative control group; (b) the chromatogram of mixed reference; (c) extraction samples.
1: Rutin; 2: Kaempferol-3-O-Rutinoside; 3: Astragalin; 4: Quercetin; 5: Kaempferol.

and in the dark. Similarly, A_i and A_j values were determined using different concentrations of VC + DPPH and VC + ethanol. Then 100 μL of DPPH solution was mixed with 100 μL of anhydrous ethanol, and the reaction was carried out at room temperature and protected from light for 10 min, and the absorbance (A_0) was measured at 517 nm as a blank control, and the above reagents were placed in a 96-well plate. The reagents listed above were placed in 96-well plates. The experiments were measured thrice in parallel, with the average values taken.

The DPPH radicals scavenging rate by the standard mixture with VC was estimated using equation (5):

$$\text{scavenging percentage } (\%) = \left(1 - \frac{A_i - A_j}{A_0}\right) \times 100\% \tag{5}$$

3. Results

3.1. Methodological investigation

Separately, 10 μL of pure methanol, a mixed control solution, and a test solution were taken using gradient elution under the chromatographic conditions described in section 2.4. As shown in Fig. 1, the results showed that the peaks of each component in the sample were separated.

The mixed control solutions 2.6, 1.8, 1.3, 0.6, and 0.05 mL under the section 2.3 were precisely pipetted into a 5 mL flask, diluted with methanol to the scale, and filtered through a 0.45 μm microporous membrane. The diluted control solution was sampled thrice for a total of 10 μL, and the linear regression was performed with the peak area of the chromatographic peak (mV/S) as the vertical coordinate (Y) and the concentration of the components in the control solution (μg/mL) as the horizontal coordinate (X). Table 1 displays the results.

The mixed control solution under section 2.3 was aspirated into the sample 10 μL at a time and repeated thrice. The peak areas of rutin, kaempferol-3-O-rutinoside, astragalin, quercetin, and kaempferol were found to be 3.91%, 2.39%, 2.45%, 2.44%, and 2.09%, respectively. The RSDs were 3.91%, 2.39%, 2.45%, 2.44%, and 2.09%, respectively, indicating that the instrument was precise.

Three samples were taken from the same batch, and the test solutions were prepared according to the operation under section 2.3, analyzed by high-performance liquid chromatography according to the operation under section 2.4 and the contents were estimated. The results demonstrated that the average extraction rates of the 5 components of rutin, kaempferol-3-O-rutinoside, astragalin, quercetin, and kaempferol were 118.88, 338.23, 28.22, 8.24, and 6.37 mg/kg and that the RSD of the average extraction rates of the 5 components were 2.45%, 2.13%, 4.75%, 4.81%, and 2.19%, respectively, indicating that the method was reproducible.

Three samples from the same batch were weighed and mixed with appropriate quantities of rutin, kaempferol-3-O-rutinoside, astragalin, quercetin, and kaempferol controls, and the test solutions were prepared according to the operation under section 2.3, detected by high-performance liquid chromatography according to the operation under section 2.4 and the contents were estimated. The recoveries for the 5 components were 101.03%, 98.49%, 97.10%, 97.56%, and 99.59%, respectively, with the RSD of 2.08%, 3.58%, 2.53%, 2.74%, and 2.47%.

The test and the mixed control solutions were obtained from the same batch and stored at room temperature for 0, 2, 4, 8, 16, and 24 h. The RSD of the control peak areas of rutin, kaempferol-3-O-rutinoside, astragalin, quercetin, and kaempferol within 24 h was 2.16%, 2.59%, 1.77%, 2.55%, and 2.27%, respectively according to the chromatographic conditions under section 2.4. The RSD of the peak areas of the control solutions for rutin, astragalin, quercetin, and kaempferol were 2.16%, 2.59%, 1.77%, 2.55%, and 2.27%; the RSD of the donor solutions' peak areas were 2.25%, 1.83%, 2.46%, 1.74%, and 1.71%, respectively. It demonstrated that the control and the test solutions were both stable within 24 h.

3.2. Single-factor experiments

The optimum range for each factor might be determined using the results of the single-factor experiments. Details were given in the Fig. A1. When the ethanol concentration was between 40% and 80%, the total extraction rate was relatively high, and it achieved a maximum when the ethanol concentration was 60%, after which it began to decrease. As a result, the ethanol concentration level was

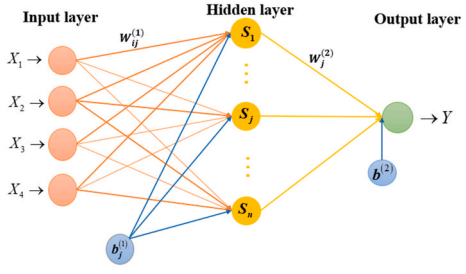

Fig. 2. Three-layer neural network structure diagram
*The input layer has four neurons, the hidden layer has n neurons, and the output layer contains one neuron.

Table 1
Linear relationships for the 4 indicator components
R^2: Goodness of Fit.

Compound	Linear equations	R^2	Linear range/μg·mL^{-1}
Rutin	Y = 12.678X+5.984	0.9980	0.53–27.56
Kaempferol-3-O-Rutinoside	Y = 12.264X+39.689	0.9980	1.55–80.34
Astragalin	Y = 14.272X+5.511	0.9992	0.16–8.32
Quercetin	Y = 20.836X+0.743	0.9990	0.08–4.16
Kaempferol	Y = 13.361X+1.126	0.9995	0.06–3.33

set to vary from 40% to 80%. When the solid-liquid ratio was between 1:15 g/mL and 1:30 g/mL, the total extraction yield took the shape of a peak. Since the total extraction yield did not vary much outside of this range, the first estimation of the solid-liquid ratio level range was 1:15 g/mL to 1:30 g/mL. When the ultrasonic duration was 45 min, the total extraction yield reached the maximum, and after 45 min, the total extraction yield began to decline. In the whole ultrasonic duration range, the total extraction yield exhibited a distinct trend of increasing and subsequently decreasing. As a result, the ultrasonic duration level was chosen to range from 30 min to 60 min. When the ultrasonic temperature was between 30 °C and 60 °C, the total extraction yield fluctuated up and down as the ultrasonic temperature increased. The total extraction yield showed great differences when the ultrasonic temperature was between 60 °C and 80 °C. As a result, the ultrasonic temperature level was chosen to vary from 60 °C to 80 °C. In the early stages, the total extraction yield varied little as the number of sieves mesh grew. The change in total extraction yield was very significant when the THR was dusty, due to the larger total contact area of the dusty particles and their ability to intercalate better with the solvent. Hence, the dusty THR was chosen for the multi-factor experiments.

In summary, the effects of ethanol concentration, solid-liquid ratio, ultrasonic duration, and ultrasonic temperature on the total extraction yield of the 5 components in THR were relatively significant. As a result, the levels of ethanol concentration, solid-liquid ratio, ultrasonic duration, and ultrasonic temperature were set to vary from 40% to 80%, 1:15 g/mL to 1:30 g/mL, 30 min–60 min and 60 °C–80 °C.

3.3. BBD experimental design protocol and results

The influencing elements were ethanol concentration (%), solid-liquid ratio (g/mL), ultrasonic duration (min), and ultrasonic temperature (°C), with the total extraction yield of the 5 components in THR serving as the response value. Using Design-Expert 8.0.6 software, a four-factor, three-level combination experiment was designed, while each group was measured thrice in parallel and the mean value taken. Table 2 presented the factors and levels, and Table 3 displayed the BBD experimental protocol and results.

3.4. Determination of the optimal extraction process

3.4.1. RSM modeling

Quadratic polynomial regression was fitted to the data in Table 2 using Design-Expert 8.0.6 software and the regression equation was obtained as follows :

$$\begin{aligned} Y = {} & 572.83 + 11.48X_1 + 9.22X_2 - 32.13X_3 + 20.88X_4 - \\ & 23.43X_1X_2 - 42.98X_1X_3 - 7.5X_1X_4 - 38.81X_2X_3 - 48X_2X_4 - \\ & 16.8X_3X_4 + 14.62{X_1}^2 - 39.22{X_2}^2 + 30.28{X_3}^2 + 36.52{X_4}^2 \end{aligned} \quad (6)$$

From the ANOVA analysis of variance in Table A1, it can be seen that $R^2 = 0.8655$, $R^2_{adj} = 0.7311$, C·V.% = 4.94%, P = 0.0006 < 0.05. Despite the overall significance of the model, six of the regression equations were tested to be insignificant, with the Lack of fit $p < 0.0001$. It stated that the model didn't truly reflect the experimental data's pattern of change and wasn't statistically significant.

3.4.2. GA-BPNN modeling

The GA toolbox of Matlab 2019a was used, with ethanol concentration (%), solid-liquid ratio (g/mL), ultrasonic duration (min),

Table 2
Factors and the levels of BBD
BBD: Box-Behnken design
A four-factor, three-level combination experiment was designed, while each group was measured thrice in parallel and the mean value taken.

Factors	Levels		
	−1	0	1
X_1 Ethanol concentration (%)	40	60	80
X_2 Solid-liquid ratio (g/mL)	15	22.5	30
X_3 Ultrasonic duration (min)	30	45	60
X_4 Ultrasonic temperature (°C)	60	70	80

Table 3
Design and results of BBD (n = 4)
BBD: Box-Behnken design
A four-factor, three-level combination experiment was conducted, while each group was measured thrice in parallel and the mean value taken.

No.	X_1	X_2	X_3	X_4	Rutin ($mg{\cdot}kg^{-1}$)	Kaempferol-3-O-Rutinoside ($mg{\cdot}kg^{-1}$)	Astragalin ($mg{\cdot}kg^{-1}$)	Quercetin ($mg{\cdot}kg^{-1}$)	Kaempferol ($mg{\cdot}kg^{-1}$)	Total extraction yield ($mg{\cdot}kg^{-1}$)	GA-BPNN prediction ($mg{\cdot}kg^{-1}$)
1	1	0	1	0	101.47 ± 2.09	411.90 ± 8.70	34.77 ± 0.94	11.40 ± 1.09	9.32 ± 0.47	568.86 ± 10.63	570.27
2	0	0	0	0	144.42 ± 36.66	376.30 ± 16.71	30.62 ± 6.88	12.55 ± 2.99	8.95 ± 1.78	572.84 ± 8.34	585.69
3	0	1	1	0	76.46 ± 5.30	353.07 ± 21.85	27.87 ± 1.98	14.43 ± 1.95	10.33 ± 1.35	482.16 ± 19.91	477.65
4	0	0	0	0	163.29 ± 8.11	355.57 ± 11.35	37.12 ± 8.83	11.08 ± 2.77	8.11 ± 1.35	575.17 ± 6.86	585.69
5	−1	0	−1	0	127.42 ± 15.16	387.75 ± 27.20	38.30 ± 4.32	8.83 ± 1.06	6.71 ± 0.56	569.01 ± 6.23	569.47
6	0	1	−1	0	165.34 ± 11.57	443.91 ± 30.65	35.71 ± 11.32	12.99 ± 2.32	9.33 ± 1.42	667.28 ± 30.82	668.82
7	0	1	0	−1	138.34 ± 13.49	401.74 ± 11.69	35.15 ± 10.43	12.79 ± 0.51	9.68 ± 1.57	597.69 ± 26.51	599.69
8	0	0	−1	1	168.07 ± 4.99	460.00 ± 10.52	45.70 ± 14.45	12.93 ± 0.31	8.67 ± 0.35	695.37 ± 24.57	696.21
9	1	−1	0	0	129.48 ± 8.49	413.37 ± 38.81	39.56 ± 11.72	15.21 ± 11.13	7.36 ± 0.93	604.97 ± 20.78	617.33
10	−1	−1	0	0	128.56 ± 6.40	352.13 ± 18.14	36.02 ± 8.02	9.78 ± 1.79	6.85 ± 1.12	533.34 ± 15.07	531.40
11	0	−1	1	0	120.65 ± 11.41	360.42 ± 43.13	30.65 ± 3.12	11.70 ± 10.10	5.07 ± 0.82	528.49 ± 36.97	529.56
12	0	0	−1	−1	116.64 ± 36.66	454.66 ± 16.45	33.62 ± 2.03	14.32 ± 1.44	10.03 ± 0.98	629.26 ± 15.69	628.94
13	0	−1	−1	0	118.53 ± 25.20	389.11 ± 19.31	34.34 ± 8.62	9.43 ± 1.72	6.94 ± 0.97	558.36 ± 34.41	557.08
14	1	1	0	0	101.93 ± 28.69	378.11 ± 6.92	34.89 ± 6.89	12.79 ± 2.54	9.75 ± 1.02	537.46 ± 28.90	536.31
15	−1	1	0	0	126.94 ± 23.48	372.74 ± 21.22	34.49 ± 8.40	14.95 ± 0.95	10.43 ± 0.46	559.56 ± 30.81	559.23
16	0	0	1	−1	141.34 ± 5.13	423.23 ± 23.23	50.64 ± 9.77	13.29 ± 0.84	10.20 ± 1.55	638.71 ± 6.22	628.76
17	1	0	−1	0	177.05 ± 12.08	480.94 ± 30.43	37.71 ± 11.77	11.60 ± 0.46	8.62 ± 0.54	715.93 ± 28.57	719.59
18	−1	0	1	0	127.71 ± 1.96	414.09 ± 5.55	32.66 ± 0.46	11.00 ± 1.01	8.39 ± 0.66	593.87 ± 6.04	594.96
19	0	0	0	0	124.62 ± 36.43	396.82 ± 13.74	28.96 ± 1.17	12.90 ± 0.81	9.22 ± 0.32	572.52 ± 36.08	585.69
20	0	0	0	0	124.45 ± 28.32	393.74 ± 16.26	29.77 ± 1.89	12.78 ± 0.78	9.34 ± 0.46	570.08 ± 7.41	585.69
21	0	0	0	0	106.56 ± 23.46	412.47 ± 14.08	32.46 ± 0.24	12.78 ± 0.83	9.24 ± 0.30	573.52 ± 29.70	585.69
22	1	0	0	−1	147.09 ± 14.94	410.35 ± 15.13	25.54 ± 6.68	15.31 ± 5.94	10.52 ± 2.74	608.81 ± 11.08	615.86
23	0	0	1	1	153.82 ± 2.75	420.31 ± 9.12	46.87 ± 1.45	9.35 ± 0.65	7.26 ± 0.44	637.60 ± 11.06	638.31
24	−1	0	0	1	144.55 ± 14.26	438.53 ± 8.02	41.29 ± 12.62	12.01 ± 1.02	8.11 ± 0.34	644.49 ± 24.58	642.92
25	−1	0	0	−1	144.30 ± 11.50	409.09 ± 9.40	37.82 ± 9.27	11.38 ± 1.33	8.07 ± 1.01	610.66 ± 20.10	625.26
26	0	1	0	1	127.97 ± 17.00	392.66 ± 22.59	35.50 ± 9.41	11.35 ± 1.47	8.14 ± 0.68	575.62 ± 36.76	575.28
27	0	−1	0	1	148.38 ± 1.32	415.24 ± 3.06	45.16 ± 0.37	9.87 ± 0.43	8.30 ± 0.56	626.95 ± 2.88	610.72
28	1	0	0	1	149.09 ±+5.16	413.19 ± 11.33	33.17 ± 11.60	9.47 ± 2.50	7.73 ± 2.18	612.65 ± 24.32	607.50
29	0	−1	0	−1	109.74 ± 5.32	291.38 ± 40.21	33.04 ± 5.65	14.33 ± 5.05	8.55 ± 1.88	457.04 ± 26.87	448.49

and ultrasonic temperature (°C) as input neurons, and total extraction yield as output neuron; 24 sets of experimental data were used as the training set and the remaining 5 sets as the testing set for model learning; the population size was set to 300, the maximum evolutionary generation was 500, the crossover probability was 0.4 and the variation probability was 0.2. Fig. 3 depicted the relationship between the number of hidden neurons and the Goodness of Fit (R^2) and Mean Square Error (MSE) after training.

When the number of hidden neurons was chosen to 4, R^2_{train}, and R^2_{test} were 0.9941 and 0.9988, respectively, indicating that the data between the testing and the training set were very closely related and that the model fits very well. MSE_{train} and MSE_{test} were 0.0131 and 0.0051, respectively, indicating that there was no overfitting, that the model was very stable, and that it could achieve the best performance. Table 4 shows the weights and thresholds of each BPNN layer when the hidden layer includes four neurons. Fig. 4 (a) depicts the link between experimental and predicted values. The distribution of all points almost formed a straight line and was located on both sides of the line. In Fig. 4 (b), the errors between the experimental and predicted values were all within ±15. Therefore, Fig. 4 showed that the model was relatively well fitted and the errors were small.

Based on the aforesaid optimization model, the total extraction yield of the 5 components was 798.35 mg/kg with an ethanol concentration of 72.8%, a solid-liquid ratio of 25.8 g/mL, an ultrasonic duration of 30.1 min, and an ultrasonic temperature of 76.1 °C. Considering the feasibility of the experimental operation, the extraction conditions were adjusted to an ethanol concentration of 73%, solid-liquid ratio1:26 g/mL, ultrasonic time of 30 min, and an ultrasonic temperature of 76.1 °C.

3.4.3. Validation experiments

Six pieces of THR powder were weighed and extracted using GA-BPNN's optimal extraction conditions. Table 5 displayed the experimental results. The difference between the experimental value and predicted values was not significant, indicating that the GA-BPNN predicted value was accurate and reliable.

3.5. Network pharmacology results for THR

Targets relating to 5 flavonoid components were collected from the TCMSP database, including 63 for kaempferol, 154 for quercetin, 21 for rutin, 2 for kaempferol-3-O-rutinoside, and 16 for astragalin, for a total of 256 targets. The Uniprot database yielded 20,375 targets for Homo sapiens, with a total of 154 target genes retrieved after annotation conversion and deduplication. Since the number of targets that could not be matched in both databases was not converted, the number of targets was lowered.

The gene cards database yielded 10,799 relevant targets, the OMIM database yielded 2 and the PharmGKB database yielded 777. The intersection of the database targets was shown in Fig. 5, and a total of 10,909 target genes were obtained after integration and deduplication.

Using the R language program, a total of 150 intersection targets for the 5 monomers and diseases were found. These targets might be considered potential targets for the 5 monomers in the treatment of oxidation-related diseases, and the Venn diagrams drawn were as follows. These genes were input into the String database, and the protein-protein interaction (PPI) analysis was performed with the lowest interaction threshold of 0.7. Subsequently, the genes were ranked by the degree value. The darker color the node is and the larger shape the node is that means the degree value is larger. The PPI network was drawn in Cytoscape_v3.9.0 software, as shown in Fig. 6, which had 140 nodes with 1666 edges.

KEGG enrichment analysis enriched a total of 199 pathways, which were sorted according to corrected p-values and the top 30 entries were selected for display. The resulting bar and bubble plots were shown in Fig. 7 (a). The pathways involving 5 flavonoid monomeric components associated with oxidation-related diseases such as the AGE-RAGE signaling pathway, lipid and atherosclerosis, tumor necrosis factor (TNF) signaling pathway, were selected as the top 15 in terms of significance and number in Fig. 7 (a).

For a total of 2363 entries, the GO enrichment analysis enriched 2139 entries for BP, 50 entries for CC, and 174 entries for MF. The top 10 entries were selected for display by sorting according to the corrected p-values. The resulting bar and bubble plots were shown in Fig. 7 (b). The 5 flavonoids were primarily involved in the metabolic process of reactive oxygen species, the response to oxidative stress, the response to reactive oxygen species, and other BPs; they participated in cell components such as membrane rafts and membrane microdomains; as well as antioxidant activity and other MFs.

Quercetin, astragalin, rutin, kaempferol, and kaempferol-3-O-rutinoside might dock with 6Y8I (fragment KCL_I013 in complex with IL-1-beta), 5F19 (the crystal structure of aspirin acetylated human cyclooxygenase-2), 6YOW (14-3-3 sigma with RelA/p65

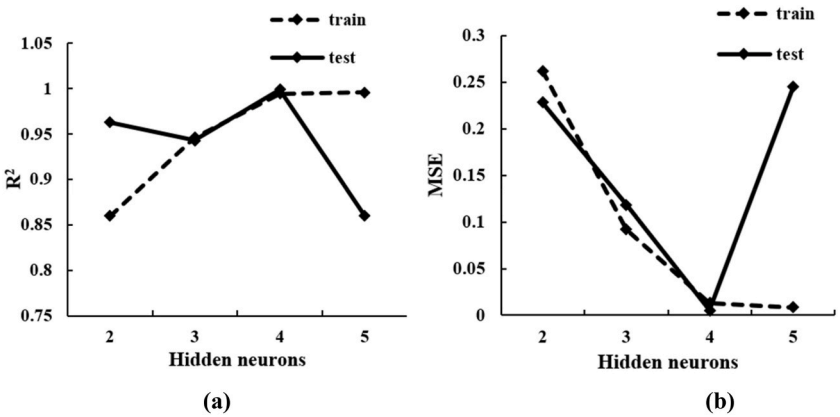

Fig. 3. The number of hidden neurons in relation to R^2 and MSE.

Table 4
GA-BPNN layer weights and thresholds
GA-BPNN: genetic algorithm-back propagation neural network
R^2: Goodness of Fit
MSE: Mean Square Error
$W^{(1)}$ and $W^{(2)}$: the network weights
$b^{(1)}$ and $b^{(2)}$: the bias values.

$W^{(1)}$				$W^{(2)}$	$b^{(1)}$	$b^{(2)}$
0.1209	9.2536	−6.4141	−0.2311	−4.2773	7.7457	2.5985
−9.7711	−4.6180	−1.5284	−9.4700	−3.0539	4.6994	/
7.4437	−7.6809	0.6802	−3.4491	−2.9134	−1.4898	/
0.5032	0.7642	−3.2329	−1.7745	5.1401	5.3869	/

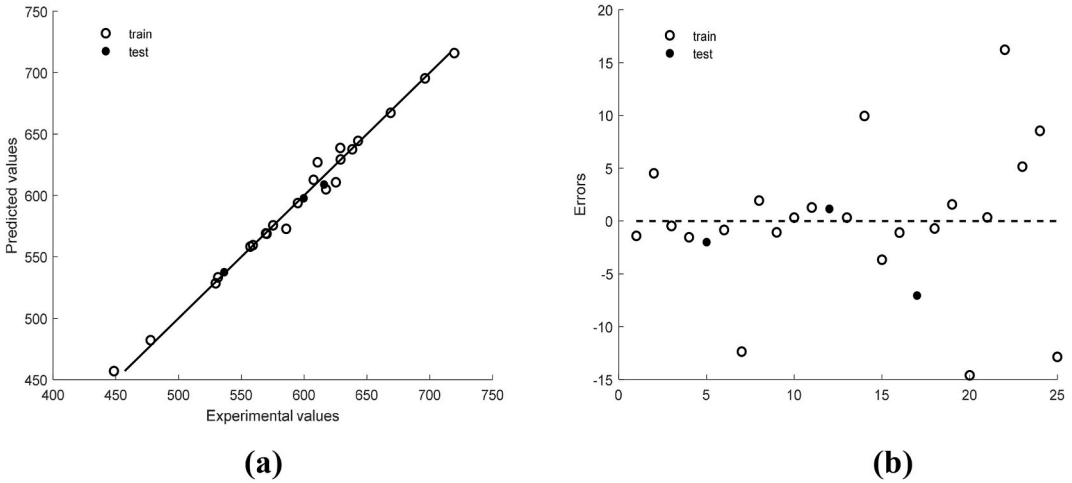

Fig. 4. Total extraction yield: (a) the relationship between predicted and experimental values; (b) residual diagram.

Table 5
Results of 6 parallel experiments
Each group was measured six times in parallel and the mean value taken. The difference between the experimental value and predicted values was not significant, indicating that the model predicted value was accurate and reliable.

Experiment number	1	2	3	4	5	6	Average
Rutin	143.03	134.09	131.64	134.52	133.17	131.14	134.59 ± 3.96
Kaempferol-3-O-rutinoside	388.42	409.31	405.75	411.39	404.91	406.72	404.42 ± 7.48
Astragalin	121.35	123.67	122.73	123.43	115.28	122.61	121.51 ± 2.88
Quercetin	82.73	71.70	73.35	73.22	81.54	79.88	77.07 ± 4.42
Kaempferol	55.67	51.30	52.21	47.35	53.50	46.39	51.07 ± 3.27
Total extraction yield (mg/kg)	791.20	790.08	785.68	789.91	788.41	786.74	788.67 ± 1.94
GA-BPNN prediction : 798.35 mg/kg							
Relative error : 1.23% < 3%							

binding site pS45 and covalently bound TCF521), 1NME (structure of casp-3 with tethered salicylate), and 5O3Y (structure of superoxide dismutase-1 bound to Ebsulfur) proteins respectively. Docking activity was distributed as follows: medium, high, high, medium, and medium. Fig. 8 depicted the molecular docking results (rutin was used as an example, the rest were put in the annex). Fig. 8 showed the bond formed by 5 components with the protein and the result obtained after filling the protein.

3.6. Antioxidant activity assay results

Pharmacological and nutritional studies demonstrated that these 5 classes of flavonoids possessed a variety of activities, such as anti-inflammatory, antioxidant, anti-bacterial, and other effects. Table 6 showed the concentration of each of the 5 components under optimal extraction conditions.

The ability of THR extracts to scavenge DPPH radicals represent the strength of their antioxidant activity. Fig. 9 depicts the DPPH scavenging rate data.

The DPPH scavenging rate gradually increased as the concentration of VC increased and eventually leveled off, as seen in the graph,

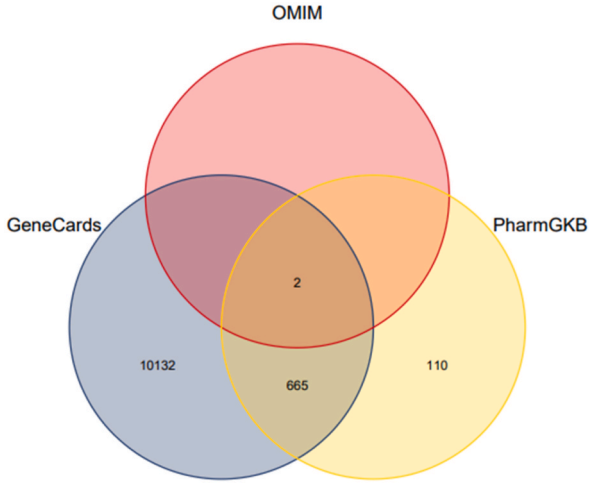

Fig. 5. Venn diagrams of oxidation-related disease targets from 3 databases.

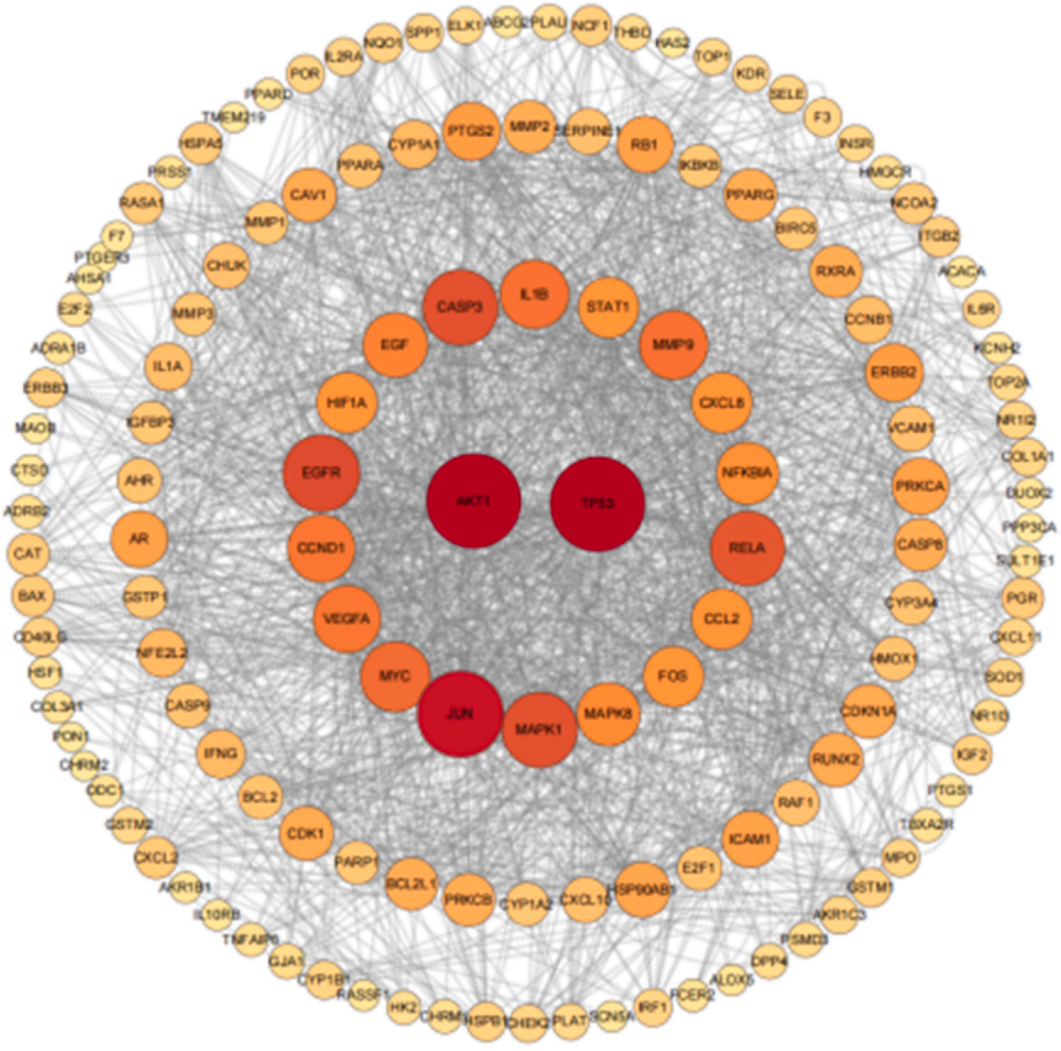

Fig. 6. PPI network diagram of the main components of THR.

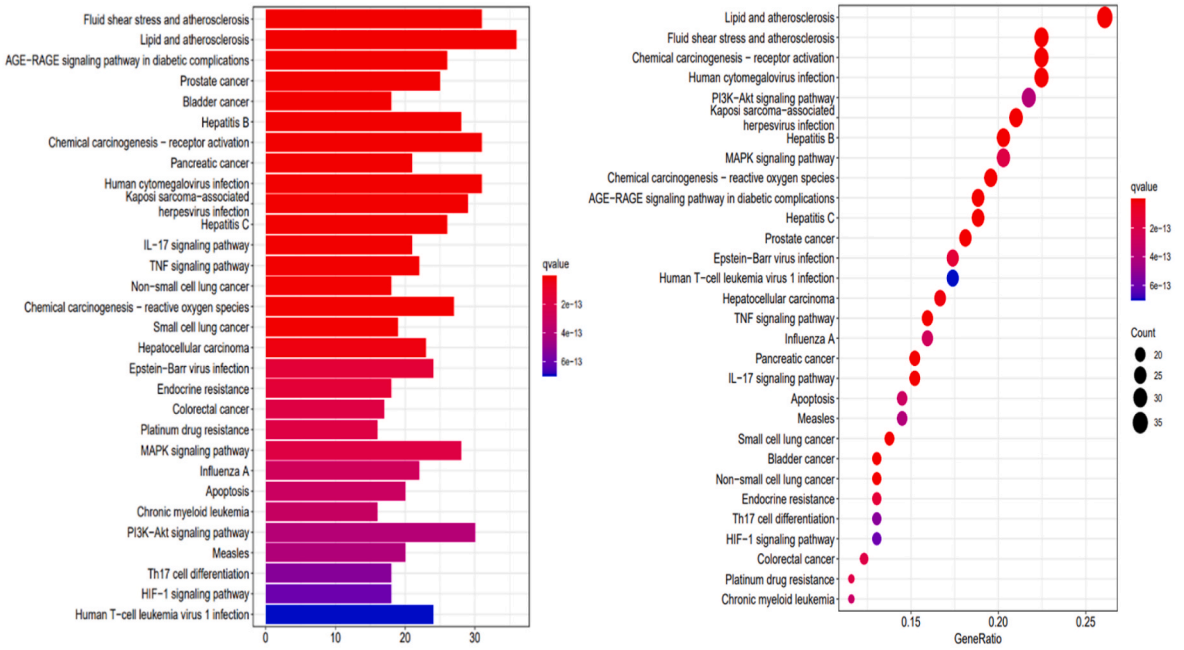

(a) KEGG enrichment analysis of THR.

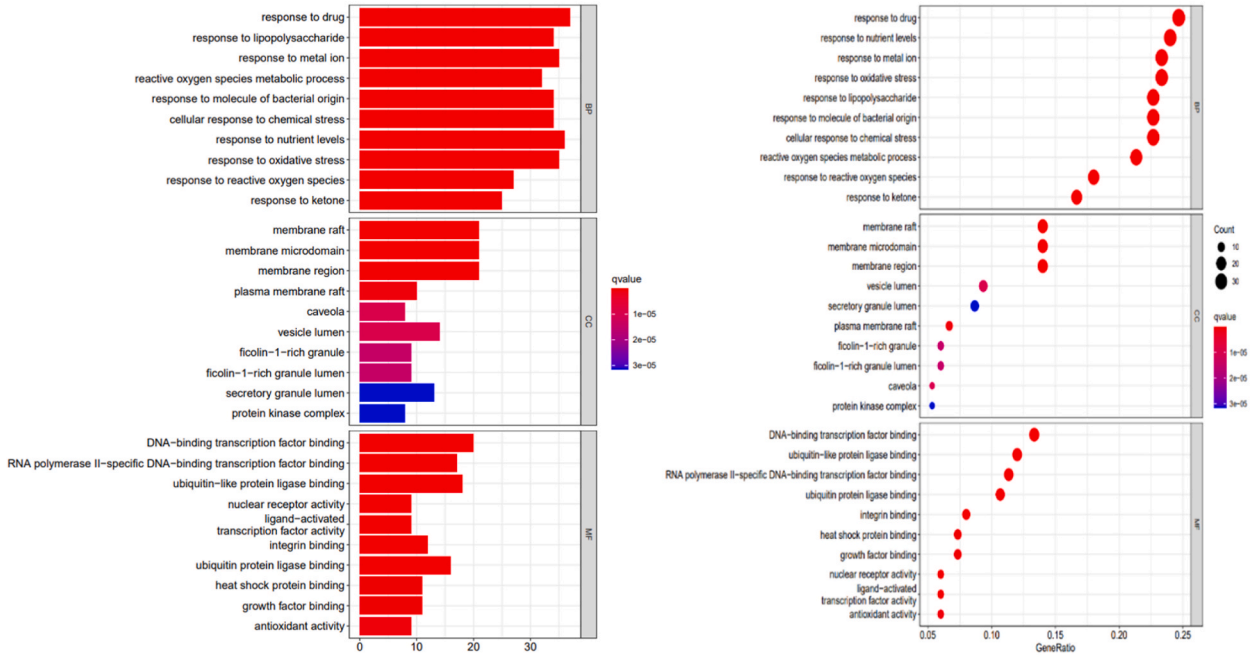

(b) GO enrichment analysis of THR.

Fig. 7. Enrichment analysis of THR: (a) KEGG enrichment analysis; (b) GO enrichment analysis
q-value: p-adjusted, is a multiple hypothesis test of p-value, which can better control the false positive rate
Count: the number of genes enriched to this KEGG/GO term in the genes input for enrichment analysis.
The color of the graph reflects the enrichment degree of differential genes in KEGG/GO term. The deeper the color (the smaller the q-value), the more significant the enrichment is, the most significant is red, followed by yellow, and colorless means that the enrichment is not significant.

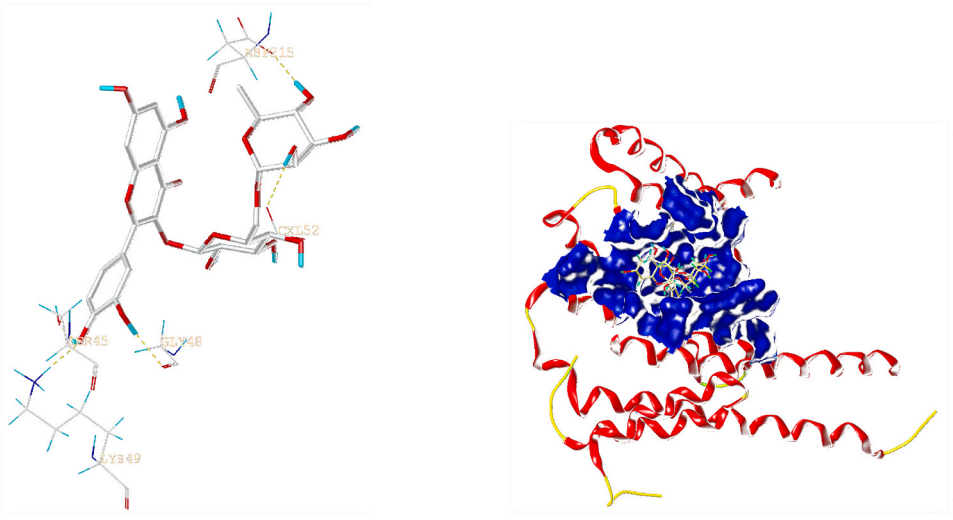

(a) rutin

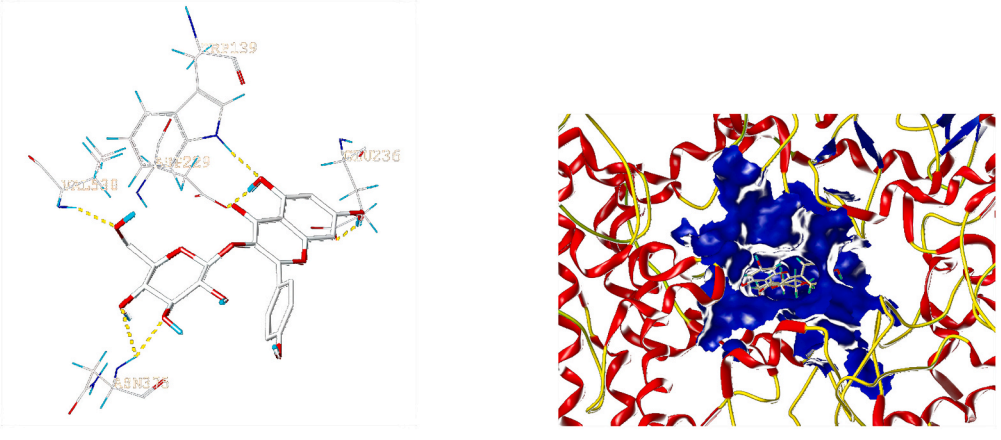

(b) Astragalin

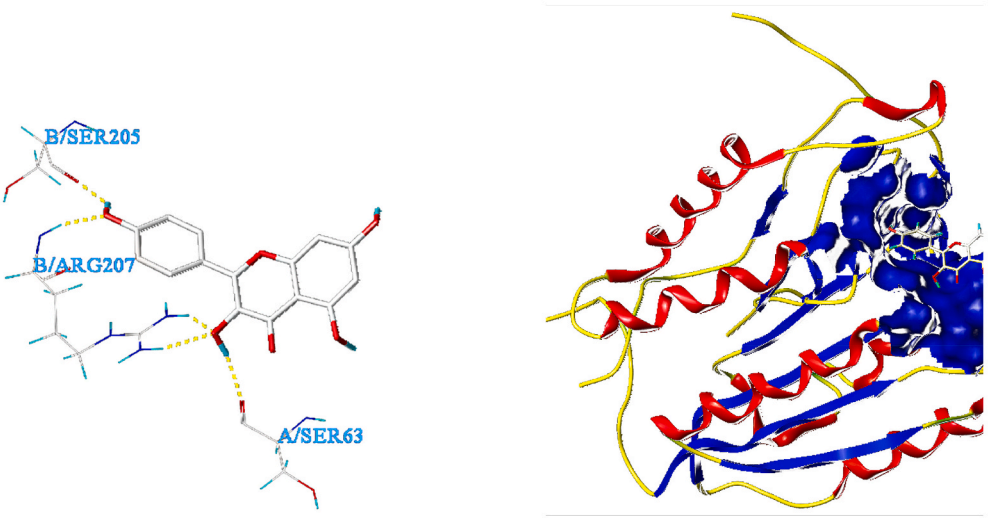

(c) Kaempferol

Fig. 8. Molecular docking results for 5 components: the bond formed by 5 components with the protein and docking diagram after filling the protein.

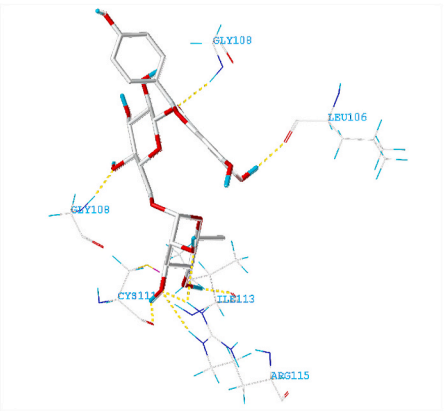

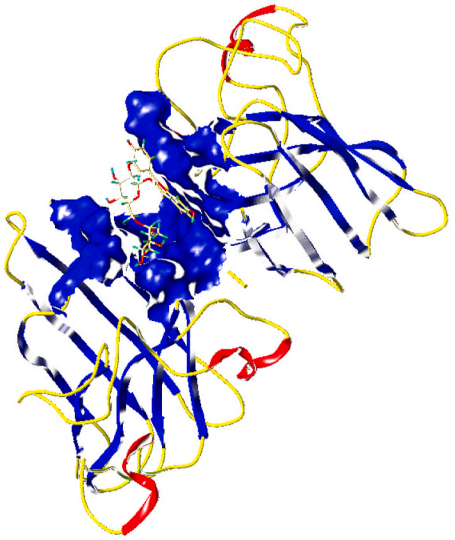

(d) Kaempferol-3-O-rutinoside

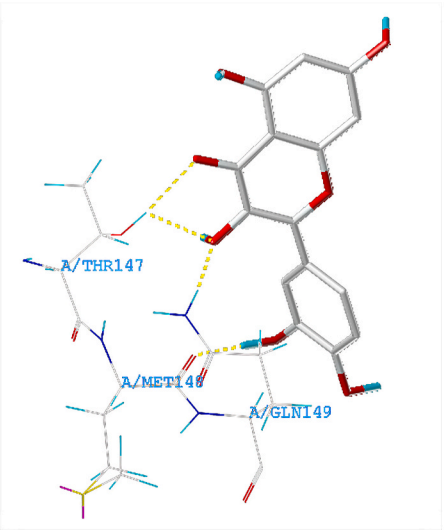

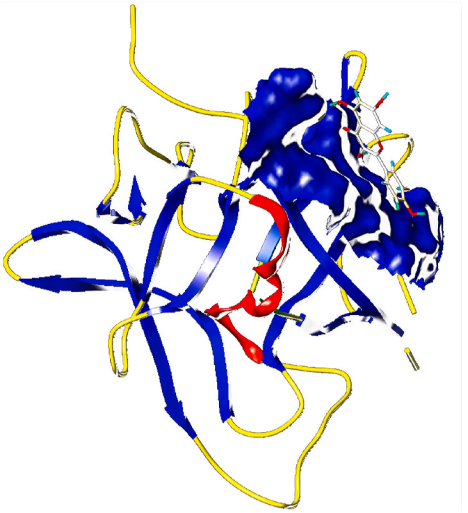

(e) Quercetin

Fig. 8. (*continued*).

and the same was true for the THR extracts. When the total concentration of five flavonoids in THR extracts was 3.033 μg/mL, the DPPH scavenging rate finally reached a maximum of 89.81%. The IC_{50} values of DPPH scavenging activity tests for THR and VC were 0.788 mg/mL and 0.1866 mg/mL, respectively. Although the THR extracts' DPPH scavenging ability was weaker than that of VC,

Table 6
Individual concentrations under the optimal conditions
The concentration of each of the 5 components (5 classes of flavonoids) under optimal extraction conditions was shown.

Reference substance	Rutin	Kaempferol-3-O-rutinoside	Astragalin	Quercetin	Kaempferol
C(μg/mL)	0.52	1.56	0.47	0.30	0.20

which was an excellent antioxidant, it was able to achieve a remarkable DPPH scavenging rate of over 70% when its concentration range was 0.758–3.033 μg/mL. This indicated that in this concentration range, the THR extracts may be an effective alternative for the antioxidant effect of traditional VC.

4. Discussion

RSM was a statistical method for solving multivariate optimization issues that employed a multiple quadratic regression equation to fit a non-linear function relationship between factors and response values and sought optimal process parameters using regression equation analysis. RSM, on the other hand, had certain limitations when it came to higher-order non-linear relationships among variables. With the development of artificial intelligence technology, some researchers applied BPNN models to optimize the extraction process of active ingredients in traditional Chinese medicine, with promising results [23]. The BPNN model, on the other hand, was extremely sensitive to the initial network weights and could easily fall into a locally optimal solution. GA was a global optimization algorithm that had good convergence and simulated the "survival of the fittest" in the biological population. As a result, the GA-BPNN model was established to optimize the neural network model's parameters using the global optimization function of the GA, to overcome the problem of local minimization of the weight convergence, to improve the model's accuracy and robustness, to make it more compatible with the highly non-linear characteristics between the extraction process conditions of traditional Chinese medicine.

The BPNN model's four input variables and one output variable constituted a super 5-dimensional surface. To further characterize the GA-BPNN model's training results and explore the sensitivity of the extracted influencing factors to the total extraction yield. The "truncation method" was employed in this work to reduce and simplify the dimensionality and visualize the reduced results. The simplified 3D surfaces of the GA-BPNN model training results were shown in Fig. 10(a–f), and the coordinate value of the highest point on each surface represented the theoretical optimal solution of the model. The optimal value of the total extraction yield trained by the model was slightly smaller than the total extraction yield at the highest point in the graphs (ethanol concentration−solid-liquid ratio, ethanol concentration−ultrasonic temperature), indicating that while the GA could find the global optimal solution for the BPNN network weights, and it sometimes only obtained a better local optimal solution for the BPNN input and output variables in the search for optimality. There was a distinct growing and decreasing trend for each surface, indicating that the experiment's four influencing factors had a significant effect on the total extraction yield. When the ultrasonic temperature, solid-liquid ratio, and ultrasonic time were close to optimal, the slope of the mountain top was relatively gentle along the ethanol concentration direction, indicating that ethanol concentration gradually tends to the optimal value. The curved surface varied significantly along the solid-liquid ratio direction in Fig. 10 (ultrasonic temperature−solid-liquid ratio, solid-liquid ratio−ethanol concentration, ultrasonic time−solid-liquid ratio), indicating that the total extraction yield was sensitive to the solid-liquid ratio.

Network pharmacology was an emerging multidisciplinary approach that used the rapid development of systems biology, bioinformatics, multidirectional pharmacology, and computer science to research the correlation between drugs and diseases holistically and systematically [24]. Network pharmacology represented a shift from traditional medicine's "one disease-one target-one drug" mentality to a cause-and-effect multi-targeted approach to the treatment of complex diseases. It effectively explained the complications of many diseases well and achieved therapeutic goals through synergistic multi-component interventions [25]. Traditional Chinese medicine has unique advantages for complex diseases due to its multi-target, multi-channel, and multi-link characteristics. Using network pharmacology to treat diseases might clearly explain the scientific principles of traditional Chinese medicine and lead to the development of novel therapeutic drugs [26].

Rutin, kaempferol-3-O-rutinoside, astragalin, quercetin, and kaempferol were 5 flavonoid components that might exhibit antioxidant effects by influencing the corresponding signaling pathways. The overproduction of reactive oxygen/nitrogen species (ROS/

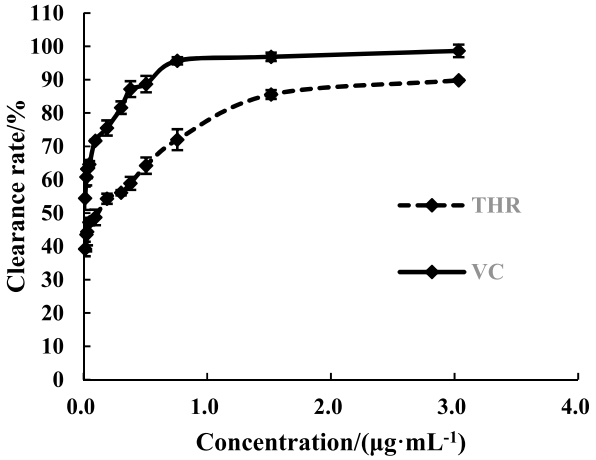

Fig. 9. Evaluation of DPPH free radical scavenging ability.

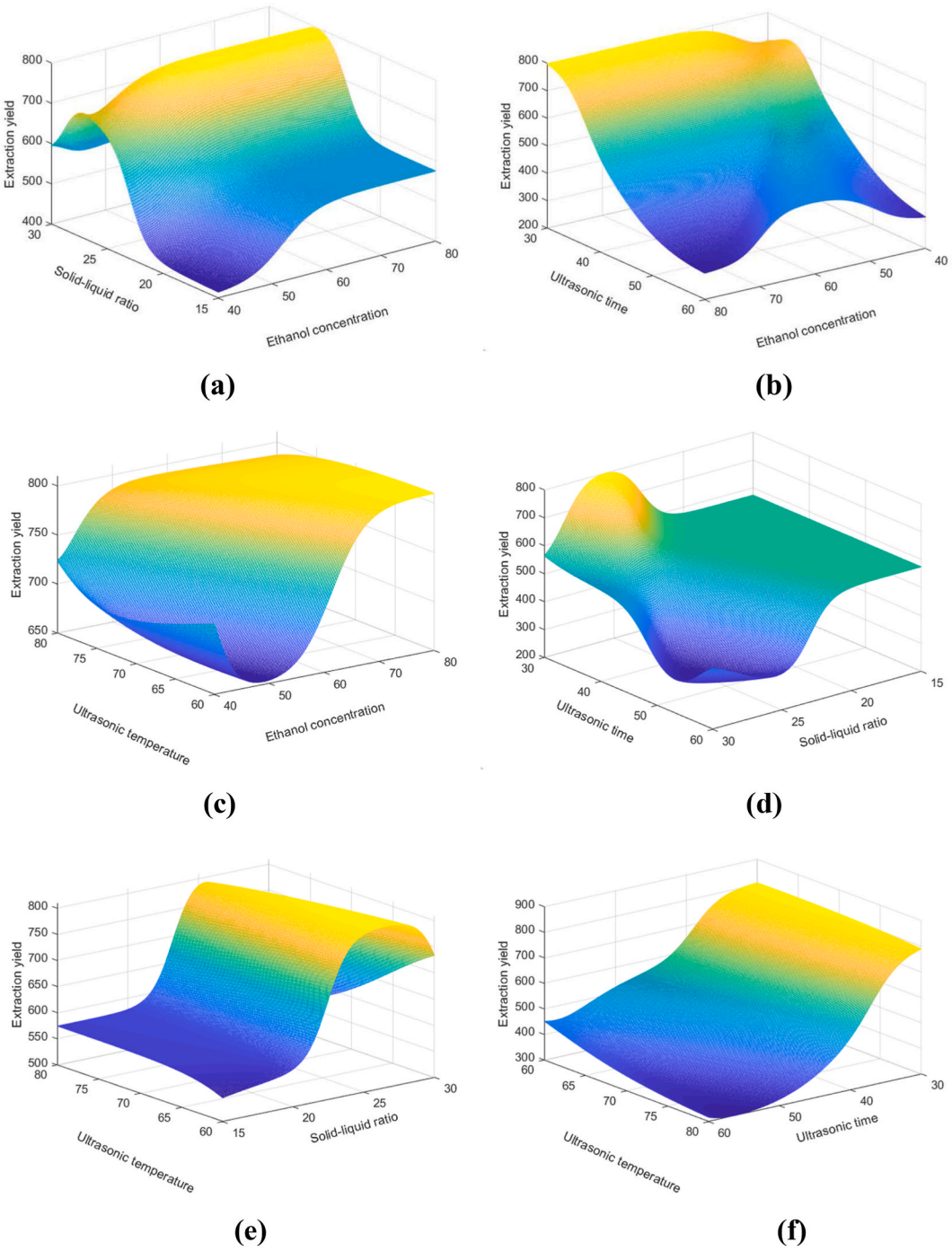

Fig. 10. Simplified 3D surface plots of a neural network (a–f): (a) ethanol concentration and solid-liquid ratio; (b) ethanol concentration and ultrasonic time; (c) ethanol concentration and ultrasonic temperature; (d) solid-liquid ratio and ultrasonic time; (e) solid-liquid ratio and ultrasonic temperature; (f) ultrasonic time and ultrasonic temperature.

RNS), such as superoxide (O_2^-), hydrogen peroxide (H_2O_2), hydroxyl radical (OH·), nitric oxide (NO), peroxynitrite ($ONOO^-$), and others, resulted in an imbalance between the pro-oxidant and the antioxidant, which was the primary cause of oxidative stress [27]. These active substances were not necessarily harmful to the body under normal physiological conditions. When they were unable to be eliminated by the body to a certain extent, the risk of diseases such as inflammation, cancer, type 2 diabetes mellitus (T2DM), and atherosclerosis increases [28,29]. The AGE-RAGE signaling pathway had been demonstrated in studies to affect the formation of reactive oxygen species *in vivo*. By affecting the AGE-RAGE signaling pathway and subsequent oxidative stress, it was possible to

prevent macrovascular complications in diabetes [30]. Oxidative stress, mediated by the production of excess reactive oxygen species, was now a common mechanism for atherosclerosis as a chronic disease [31]. According to Fig. 10, the 5 components might impact the atherosclerotic process by acting on the lipid and atherosclerosis pathways. In addition, the 5 flavonoid components of THR have been associated with the oxidative stress-induced TNF signaling pathway. TNF was a multifunctional cytokine that induced cell death via receptor-mediated caspase activation and mitochondrial dysfunction [32].

Numerous authors have explored the effects of the THR polysaccharides and phenols on oxidative stress *in vivo*. For instance, enzymolysis-ultrasonic assisted extraction (EUAE) was used to extract TDGP-3, a new polysaccharide with the potential to alleviate hyperlipidemia and prevent oxidative stress, primarily by regulating blood lipid (TC, TG, HDL-C, LDL-C) levels and restoring the activity of liver antioxidant enzymes (SOD, GSH-Px, CAT) [33]. *In vitro*, another study [34] demonstrated that THR polysaccharides had a concentration-dependent ability to scavenge hydroxyl radicals (OH·), superoxide (O_2^-), and chelate ferrous ions in addition to DPPH; whereas *in vivo*, it reduced intracellular ROS levels, decreased catalase (CAT) and superoxide dismutase (SOD) activities, increased lactate dehydrogenase (LDH) activity, and increased malondialdehyde (MDA) levels, thus protecting the antioxidant activity of RAW264.7 cells. Sun [35] found that THR phenolic extract could inhibit tumor growth by regulating the expression of Bcl-2 family proteins and activating caspase family proteins. This inhibited tumor growth while increasing interleukin-2 levels, TNF-α production, and $CD4^+/CD8^+$ ratio while decreasing malondialdehyde (MDA) content in the THR group of mice, demonstrating that THR phenolics could prevent tumorigenesis through immune function and antioxidant activity.

Flavonoids were antioxidant active substance representatives. The phenolic hydroxyl groups in the flavonoid structure were good radical electron donors and free radical scavengers from a structural standpoint [36]. Furthermore, the carbonyl group in the structure stabilized the phenoxy group during the interaction of flavonoids with free radicals via aromatic ring resonance [37]. Hu [38] studied the flavonoids in Folium Artemisiae Argyi (FAA) and confirmed their antioxidant activity against *C. elegans*, which might be regulated by the insulin/insulin-like growth factor-1 (IGF-1) signaling pathway. Parhiz [39] studied the flavonoids in Hesperidin (Hsd) and its aglycone, Hesperetin (Hst) flavonoids, and found that the antioxidant activity of Hsd/Hst was not limited to free radical scavenging but also enhances antioxidant cellular defense via ERK/Nrf2 signaling pathway. However, no one has investigated the mechanism and detailed process of flavonoids in THR *in vivo* against oxidative stress. The network pharmacology of 5 flavonoid components was investigated in this study to provide the relationship between the AGE-RAGE signaling pathway, lipid and atherosclerosis, TNF signaling pathway, and reactive oxygen species *in vivo*, and to provide a basis for subsequent experimental studies of THR flavonoids *in vivo*. It pointed the way forward for further research on the antioxidant activity of THR flavonoids *in vivo*.

THR is an edible plant with low toxic side effects that are widely utilized in daily life as dietary supplements, health food, and nutritional products. Its active ingredients, such as flavonoids, polyphenols, and polysaccharides, may anti-oxidative stress in humans. Furthermore, THR is a "plant antibiotic" that cannot be replaced by drugs due to its unique efficacy on various fever and edema, and it was often used in clinical practice in combination with other drugs to achieve significant clinical efficacy. THR development and usage as a traditional medicine with good biological value has a broad prospect, which is conducive to the development of traditional Chinese medicine foods, traditional Chinese medicine pharmaceuticals, proprietary Chinese medicine industries and others.

5. Conclusion

In the research, the GA-BPNN was used to investigate the optimal extraction process of 5 flavonoid components in THR: kaempferol, quercetin, rutin, kaempferol-3-O-rutinoside, and astragalin, based on BBD. The total extraction yield was maximum when the ethanol concentration was 73%, the solid-liquid ratio was 1:26 g/mL, the ultrasonic duration was 30 min, and the ultrasonic temperature was 76 °C. The total extraction yield of the 5 components was confirmed to be 788.67 mg/kg at this process condition, and the relative error with the model prediction was 1.23%, indicating that the GA-BPNN method for optimizing the extraction process of active ingredients in THR was accurate and reliable. The potential molecular mechanisms of these 5 flavonoid components for the treatment of oxidative diseases were predicted using network pharmacology, and the molecular docking scores of the 5 monomeric components, quercetin, astragalin, rutin, kaempferol, and kaempferol-3-O-rutinoside, were obtained as 3.63, 7.52, 6.93, 3.37, and 4.40 respectively. Finally, the antioxidant activity of the THR extracts under the optimal extraction process conditions was examined using DPPH. The total concentration of the 5 monomeric components in THR extracts was 3.033 μg/mL, and the DPPH radical's scavenging rate was 89.81%, indicating that they have good antioxidant ability.

In summary, we have highlighted the efficacy of the GA-BPNN optimization method for enhancing the extraction process of active components in THR. Furthermore, the integration of network pharmacology models and *in vitro* DPPH assays has substantiated the antioxidative properties of all five monomeric components, both *in vivo* and *in vitro*.

Author contribution statement

J. Song and X. Li conceived and designed the experiments; J. Shu and Y. Zhou wrote the paper; Y. Zhao and Y. Zhou performed the experiments; J. Shu and F. Lin contributed reagents, materials, analysis tools or data and analyzed and interpreted the data;. All authors have read and agreed to the published version of the manuscript.

Funding

This research was jointly supported by the Education Science Planning Project of Zhejiang Province (No.2022SCG428), Zhejiang Provincial Natural Science Foundation (No.LY22H270002), Zhejiang Provincial Science and Technology Project of Traditional

Chinese Medicine (No.2023ZF059).

Table A1
Results of analysis of variance (ANOVA) about Box–Behnken design (BBD)
* Level of significance: *p < 0.05, **p < 0.01, ***p < 0.001.

Source	Sum of Squares	df	Mean Square	F-Value	P-Value
model	76695.90	14	5478.28	6.44	0.0006***
A-solid-liquid ratio	1581.22	1	1581.22	1.86	0.1944
B-ethanol concentration	1020.13	1	1020.13	1.20	0.2920
C-ultrasonic time	12385.70	1	12385.70	14.55	0.0019**
D-ultrasonic temperature	5229.83	1	5229.83	6.15	0.0265*
AB	2195.60	1	2195.60	2.58	0.1305
AC	7388.74	1	7388.74	8.68	0.0106*
AD	224.76	1	224.76	0.26	0.6153
BC	6025.63	1	6025.63	7.08	0.0186*
BD	9214.37	1	9214.37	10.83	0.0054**
CD	1129.21	1	1129.21	1.33	0.2686
A^2	1385.68	1	1385.68	1.63	0.2227
B^2	9977.77	1	9977.77	11.73	0.0041**
C^2	5946.3	1	5946.3	6.99	0.0193*
D^2	8652.22	1	8652.22	10.17	0.0066**
Residual	11913.70	14	850.98	–	–
Lack of Fit	11900.12	10	1190.01	350.36	<0.0001***
Pure Error	13.59	4	3.40	–	–
Cor Total	88609.61	28	–	–	–

*Level of significance: *$p < 0.05$, **$p < 0.01$, ***$p < 0.001$.
Critical value (C·V.): $F_{0.05}(1, 14) = 4.60$, $F_{0.01}(1, 14) = 8.86$.

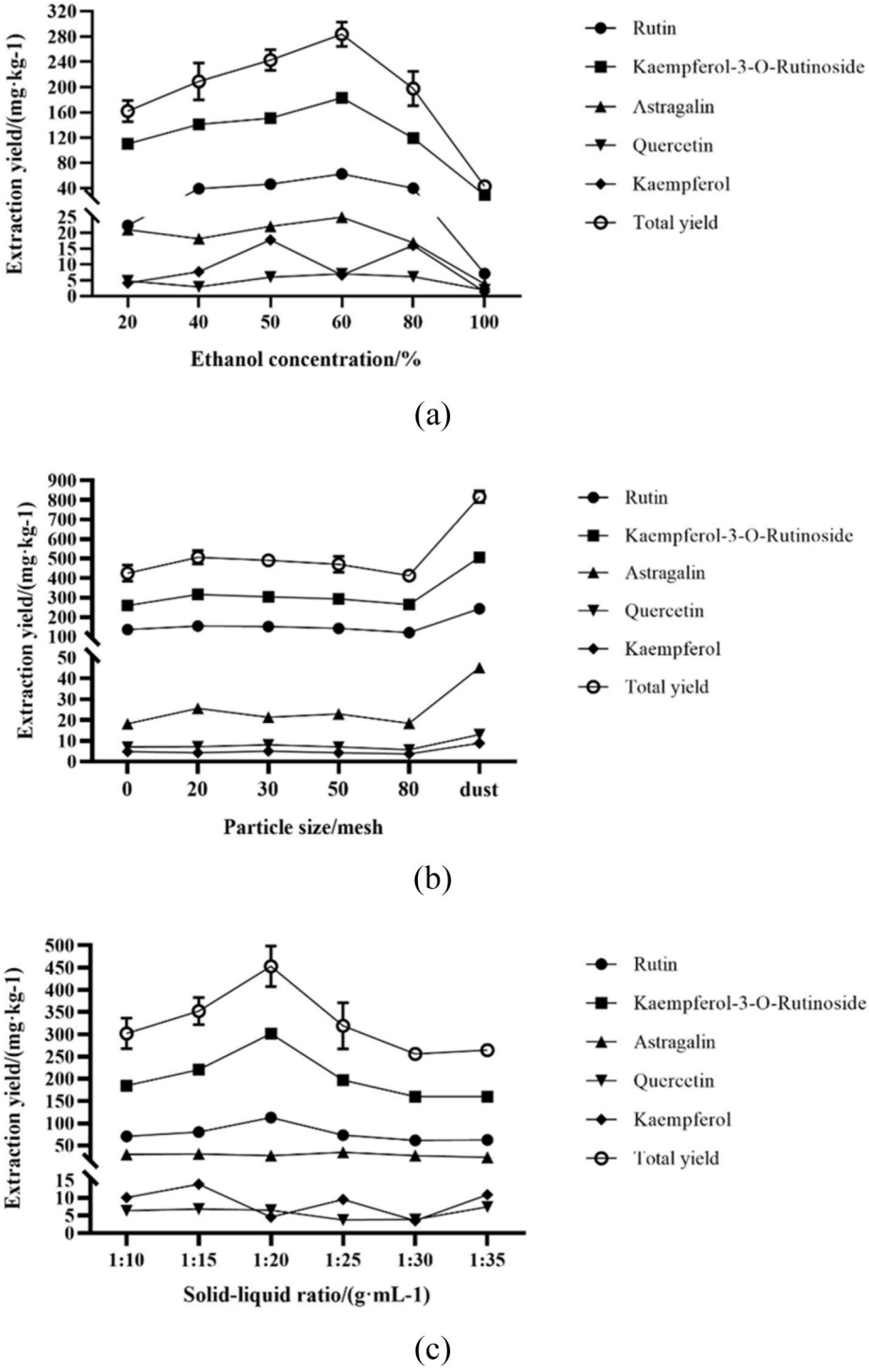

Fig. A1. Results of single-factor experiment

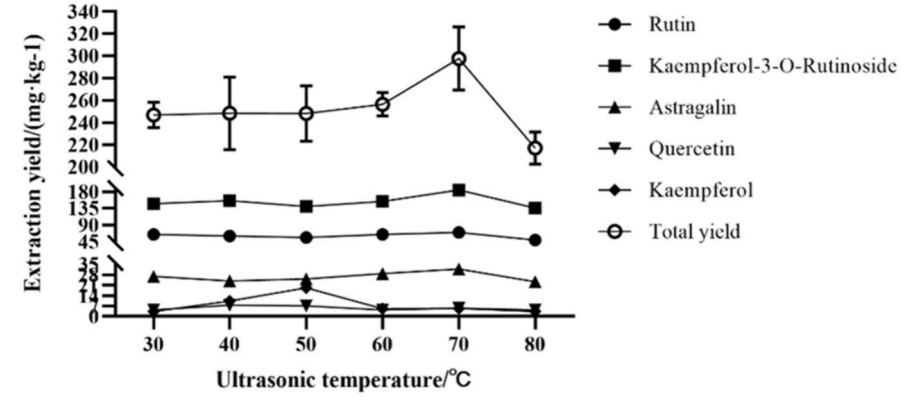

(d)

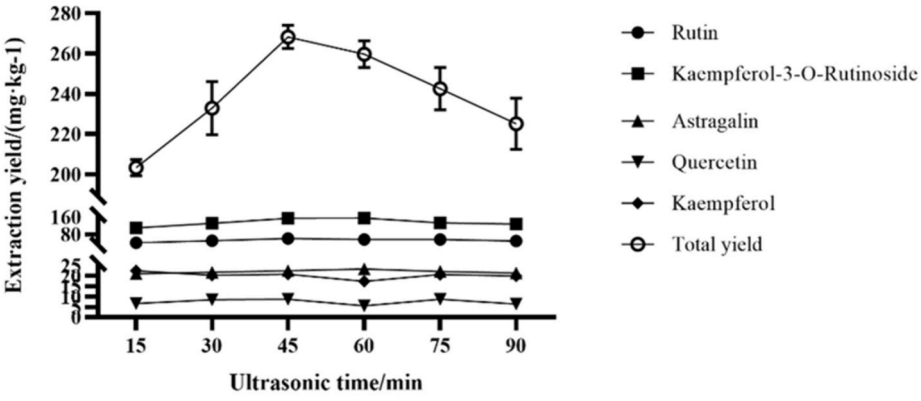

(e)

Fig. A1. (*continued*).

Declaration of competing interest

The authors declare that they have no known competing financial interests or personal relationships that could have appeared to influence the work reported in this paper.

References

[1] S. Andres, S. Pevny, R. Ziegenhagen, N. Bakhiya, B. Schäfer, K.I. Hirsch-Ernst, A. Lampen, Safety aspects of the use of quercetin as a dietary supplement, Mol. Nutr. Food Res. 62 (1) (2018).
[2] Z. Huang, Q. Mao, J. Wei, Evaluation of anti-inflammatory, analgesic and antipyretic actions for the extracts from Radix Tetrastigmae, Chinese New Drugs Journal (7) (2005) 861–864.
[3] T. Ji, W.W. Ji, J. Wang, H.J. Chen, X. Peng, K.J. Cheng, D. Qiu, W.J. Yang, A comprehensive review on traditional uses, chemical compositions, pharmacology properties and toxicology of Tetrastigma hemsleyanum, J. Ethnopharmacol. 264 (2021), 113247.
[4] Z. Feng, W. Hao, X. Lin, D. Fan, J. Zhou, Antitumor activity of total flavonoids from Tetrastigma hemsleyanum Diels et Gilg is associated with the inhibition of regulatory T cells in mice, OncoTargets Ther. 7 (2014) 947–956.
[5] W. Ji, X. Peng, T. Lou, J. Wang, W. Qiu, Total flavonoids from Tetrastigma hemsleyanum ameliorates inflammatory stress in concanavalin A-induced autoimmune hepatitis mice by regulating Treg/Th17 immune homeostasis, Inflammopharmacology 27 (6) (2019) 1297–1307.
[6] J. Silva Dos Santos, J.P. Goncalves Cirino, P. de Oliveira Carvalho, M.M. Ortega, The pharmacological action of kaempferol in central nervous system diseases: a review, Front. Pharmacol. 11 (2020), 565700.
[7] N. Sharma, S. Biswas, N. Al-Dayan, A.S. Alhegaili, M. Sarwat, Antioxidant role of kaempferol in prevention of hepatocellular carcinoma, Antioxidants 10 (9) (2021).
[8] X. Wang, Y. Yang, Y. An, G. Fang, The mechanism of anticancer action and potential clinical use of kaempferol in the treatment of breast cancer, Biomed. Pharmacother. 117 (2019), 109086.
[9] Y.H. Rahul, Siddique, neurodegenerative diseases and flavonoids: special reference to kaempferol, CNS Neurol. Disord.: Drug Targets 20 (4) (2021) 327–342.
[10] F. Babaei, M. Mirzababaei, M. Nassiri-Asl, Quercetin in food: possible mechanisms of its effect on memory, J. Food Sci. 83 (9) (2018) 2280–2287.
[11] W.M. Dabeek, M.V. Marra, Dietary quercetin and kaempferol: bioavailability and potential cardiovascular-related bioactivity in humans, Nutrients 11 (10) (2019).
[12] G. Derosa, P. Maffioli, A. D'Angelo, F. Di Pierro, A role for quercetin in coronavirus disease 2019 (COVID-19), Phytother Res. 35 (3) (2021) 1230–1236.
[13] S.K. Wong, K.-Y. Chin, S. Ima-Nirwana, Quercetin as an agent for protecting the bone: a review of the current evidence, Int. J. Mol. Sci. 21 (17) (2020).

[14] B. Gullón, T.A. Lú-Chau, M.T. Moreira, J.M. Lema, G. Eibes, Rutin: a review on extraction, identification and purification methods, biological activities and approaches to enhance its bioavailability, Trends Food Sci. Technol. 67 (2017) 220–235.
[15] Y. Li, X. Yu, Y. Wang, X. Zheng, Q. Chu, Kaempferol-3-O-rutinoside, a flavone derived from Tetrastigma hemsleyanum, suppresses lung adenocarcinoma via the calcium signaling pathway, Food Funct. 12 (18) (2021) 8351–8365.
[16] Y. Ma, Y. Liu, A. Sun, Y. Du, M. Ye, X. Pu, X.J.R.a. Qi, Intestinal absorption and neuroprotective effects of kaempferol-3-, O-rutinoside 7 (50) (2017) 31408–31416.
[17] Y. Wang, C. Tang, H. Zhang, Hepatoprotective effects of kaempferol 3-O-rutinoside and kaempferol 3-O-glucoside from Carthamus tinctorius L. on CCl4-induced oxidative liver injury in mice, J. Food Drug Anal. 23 (2) (2015) 310–317.
[18] A. Riaz, A. Rasul, G. Hussain, M.K. Zahoor, F. Jabeen, Z. Subhani, T. Younis, M. Ali, I. Sarfraz, Z. Selamoglu, Astragalin: a bioactive phytochemical with potential therapeutic activities, Adv. Pharmacol. Sci. 2018 (2018), 9794625.
[19] Q. Shao, Y. Deng, H. Shen, H. Fang, X. Zhao, Optimization of polysaccharides extraction from Tetrastigma hemsleyanum Diels et Gilg using response surface methodology, Int. J. Biol. Macromol. 49 (5) (2011) 958–962.
[20] C. Li, Y. Cui, J. Lu, C. Liu, S. Chen, C. Ma, Z. Liu, J. Wang, W. Kang, Ionic liquid-based ultrasonic-assisted extraction coupled with HPLC and artificial neural network analysis for ganoderma lucidum, Molecules 25 (6) (2020).
[21] S. Xu, H. Wan, X. Zhao, Y. Zhang, J. Yang, W. Jin, Y. He, Optimization of extraction and purification processes of six flavonoid components from Radix Astragali using BP neural network combined with particle swarm optimization and genetic algorithm, Ind. Crop. Prod. 178 (2022), 114556.
[22] L. Yu, W. Jin, X. Li, Y. Zhang, Optimization of bioactive ingredient extraction from Chinese herbal medicine Glycyrrhiza glabra: a comparative study of three optimization models, Evid. Based Complement Alternat. Med. (2018), 6391414, 2018.
[23] L. Yu, W. Jin, J. Zhou, X. Li, Y. Zhang, Optimal extraction bioactive components of tetramethylpyrazine in Chinese herbal medicine jointly using back propagation neural network and genetic algorithm in R language, Pak. J. Pharm. Sci. 33 (1) (2020) 95–102.
[24] R. Zhang, X. Zhu, H. Bai, K. Ning, Network pharmacology databases for traditional Chinese medicine: review and assessment, Front. Pharmacol. 10 (2019) 123.
[25] C. Nogales, Z.M. Mamdouh, M. List, C. Kiel, A.I. Casas, H.H.H.W. Schmidt, Network pharmacology: curing causal mechanisms instead of treating symptoms, Trends Pharmacol. Sci. 43 (2) (2022) 136–150.
[26] Z. Zhou, B. Chen, S. Chen, M. Lin, Y. Chen, S. Jin, W. Chen, Y. Zhang, Applications of network pharmacology in traditional Chinese medicine research, Evid. Based Complement Alternat. Med. 2020 (2020), 1646905.
[27] X. Li, Y. Zhang, Y. Yuan, Y. Sun, Y. Qin, Z. Deng, H. Li, Protective effects of selenium, vitamin E, and purple carrot anthocyanins on D-galactose-induced oxidative damage in blood, liver, heart and kidney rats, Biol. Trace Elem. Res. 173 (2) (2016) 433–442.
[28] R. Apak, M. Özyürek, K. Güçlü, E. Çapanoğlu, Antioxidant activity/capacity measurement. 1. Classification, physicochemical principles, mechanisms, and electron transfer (ET)-Based assays, J. Agric. Food Chem. 64 (5) (2016).
[29] F. Ito, Y. Sono, T. Ito, Measurement and clinical significance of lipid peroxidation as a biomarker of oxidative stress: oxidative stress in diabetes, atherosclerosis, and chronic inflammation, Antioxidants 8 (3) (2019).
[30] Z. Wang, J. Zhang, L. Chen, J. Li, H. Zhang, X. Guo, Glycine suppresses AGE/RAGE signaling pathway and subsequent oxidative stress by restoring Glo1 function in the aorta of diabetic rats and in HUVECs, Oxid. Med. Cell. Longev. (2019), 4628962, 2019.
[31] A.J. Kattoor, N.V.K. Pothineni, D. Palagiri, J.L. Mehta, Oxidative stress in atherosclerosis, Curr. Atherosclerosis Rep. 19 (11) (2017) 42.
[32] H. Sone, H. Akanuma, T. Fukuda, Oxygenomics in environmental stress, Redox Rep. 15 (3) (2010) 98–114.
[33] Y. Ru, X. Chen, J. Wang, L. Guo, Z. Lin, X. Peng, B. Qiu, Polysaccharides from Tetrastigma hemsleyanum Diels et Gilg: extraction optimization, structural characterizations, antioxidant and antihyperlipidemic activities in hyperlipidemic mice, Int. J. Biol. Macromol. 125 (2019) 1033–1041.
[34] Q. Huang, W. He, I. Khudoyberdiev, C.L. Ye, Characterization of polysaccharides from Tetrastigma hemsleyanum Diels et Gilg Roots and their effects on antioxidant activity and H2O2-induced oxidative damage in RAW 264.7 cells, BMC Chem. 15 (1) (2021) 9.
[35] Y. Sun, R. Tsao, F. Chen, H. Li, H. Peng, L. Jiang, Y. Chen, Z. Deng, The phenolic profiles of Radix Tetrastigma after solid phase extraction (SPE) and their antitumor effects and antioxidant activities in H22 tumor-bearing mice, Food Funct. 8 (11) (2017) 4014–4027.
[36] I. Gulcin, Antioxidant activity of food constituents: an overview, Arch. Toxicol. 86 (3) (2012) 345–391.
[37] K.E. Heim, A.R. Tagliaferro, D.J. Bobilya, Flavonoid antioxidants: chemistry, metabolism and structure-activity relationships, J. Nutr. Biochem. 13 (10) (2002) 572–584.
[38] Q. Hu, Z. Liu, Y. Guo, S. Lu, H. Du, Y. Cao, Antioxidant capacity of flavonoids from Folium Artemisiae Argyi and the molecular mechanism in Caenorhabditis elegans, J. Ethnopharmacol. 279 (2021), 114398.
[39] H. Parhiz, A. Roohbakhsh, F. Soltani, R. Rezaee, M. Iranshahi, Antioxidant and anti-inflammatory properties of the citrus flavonoids hesperidin and hesperetin: an updated review of their molecular mechanisms and experimental models, Phytother Res. 29 (3) (2015) 323–331.